ISSN 1330-3651 (Print), ISSN 1848-6339 (Online)
UDC/UDK 677.027.625.55:504.064]:004.94

# SIMULATION OF PERIODIC NANOSTRUCTURES FABRICATED BY MULTI-BEAM INTERFERENCE OF AN ULTRA-SHORT PULSE LASER

*Robert Pospichal, Gerhard Liedl*

Original scientific paper

During the last years, the self-cleaning surface structures of lotus flowers have been reproduced in numerous ways on textiles or paintings and other surfaces to reduce sensitivity against pollution which, in turn, allows a reduction of water- and detergent consumption. Unfortunately, some of these techniques suffer from wear or are potentially biohazardous due to the small particle size. We present a method to produce nanostructures on surfaces by multi-beam interference of ultra-short laser pulses. Expected intensity distributions, as well as ablation rates of various configurations have been simulated and show the feasibility of the suggested process.

***Keywords:*** *lotus-effect, multi-beam interference, nano-structures, ultra-short pulse laser*

## Simulacija periodičnih nanostruktura dobivenih interferencijom multi snopa lasera ultra kratkog impulsa

Izvorni znanstveni članak

Tijekom proteklih godina površinske strukture lotosova cvijeta s karakteristikom samočišćenja na mnogo su raznih načina reproducirane na tkaninama ili slikama i drugim površinama kako bi se smanjila osjetljivost na zagađivanje, što zatim omogućuje smanjenje potrošnje vode i deterdženta. Nažalost, neke od tih metoda trpe od zamora ili su potencijalno biološki štetne zbog malih dimenzija čestica. Mi prikazujemo metodu proizvodnje nanostruktura na površinama interferencijom multi-snopa ultra kratkih impulsa lasera. Simulirani su očekivani intenziteti raspodjele kao i iznosi odnošenja raznih konfiguracija te pokazana izvedivost predloženog postupka.

***Ključne riječi:*** *interferencija multi snopom, laser s ultra kratkim impulsima, lotosov efekt, nanostruktura*

## 1 Introduction

### 1.1 Lotus-effect

Lotus-effect is the self-cleaning ability of natural surfaces. It is named by Barthlott und Neinhuis [1] after the Lotus-plant, which shows selfsame characteristics. Nearly every ecosystem contains examples of this lotus-effect. Neinhuis and Barthlott did a very complete listing of the natural occurrences [1, 2].

The effect is based on two principles [3]:

Examples in nature show a hydrophobic surface, the so called cuticula, which consists in most cases of wax. This layer increases the interface tension between the leaf and the water droplet. As a consequence, the contact angle between surface and water droplet increases, too. It has been shown that it is possible that such wax layers may erode during plant growth, leaving plant surfaces almost smooth and without water-repellent properties [1].

The other main effect is based on the two-part surface structure:

Burlings (papillae) are placed on the cuticula. The burlings extend to a height up to 5 μm or 10 μm and are placed at a distance between 10 μm and 15 μm next to each other. These papillae exhibit finer structures on their surfaces, where the actual nano-structure is superimposed by means of wax crystals. Usually, these crystals show diameters in the order of 100 nm [1].

Several studies have proved that a correlation exists between the existence of a two-part surface structure and the super-hydrophobic behaviour. On the other hand, it has been shown that examples in nature exist, which exhibit one-part surface structures in the nanometer range with excellent super-hydrophobic behaviour [4, 5].

In any case, the contact area between water droplet and surface is minimized as well as adhesive forces. As a consequence, water droplets on the surface take a more or less spherical from.

### 1.2 Environmental impact

It is clear that hydrophobic surfaces where pollutants can be removed easily or do not adhere at all have the potential to reduce usage of detergents dramatically. On the other hand, production processes of hydrophobic surfaces will influence the environment, too.

The expected impact can be divided in two main parts: First of all, usage of materials which exhibit a lotus-effect will definitely influence the environment. Additionally, production processes with their unknown threats to environmental contamination have to be evaluated thoroughly. The process proposal presented here has a chance to influence both.

#### 1.2.1 Environmental impact of the lotus-effect

The self-cleaning ability of surfaces will of course result in a reduced number of cleaning processes. The lotus-effect itself does not depend on any detergents. Therefore, water consumption as well as detergent consumption can be decreased substantially. Furthermore, in the case of outdoor applications where surfaces will be cleaned by rain water it is supposable that cleaning processes can be skipped completely.

The first stage of the presented project aims to produce plastic films with this self-cleaning ability. In further stages it is also planned to adapt the process to textile structures or even fibres. It is intended that the required structures should be produced by means of an ultra-short laser system.

In principle, the structuring of almost any material should be possible. Prior to that, a thorough

understanding of the impact of different features and their shape and size is required. Additionally, an adequate laser source with sufficient pulse energy and duration and frequency is needed.

### 1.2.2 Environmental impact of the process

The conventional way of a hydrophobic finishing - for example for textiles - is a treatment with hydrophobic particles like fluorocarbons or silicon oils [6]. Such processes suffer from some disadvantages:

- wash resistance of the finish is very limited or can just be guaranteed with large expenses [6]
- used chemicals are critical from both ecological and biological point of view [7]
- need of an own process, in case of textiles after the fibre production or after the textile assembly.

Therefore some environmental issues can be avoided if the lotus-effect is used instead of conventional chemicals. Most existing lotus-effect applications rely on a coating of the textile with a finish which contains the nano-particles.

Although no chemicals like fluorocarbons or silicon oils are needed any more, the nano-coating itself is also not harmless, especially handling of the dry coating can be hazardous.

The danger originates from the particles itself. Due to the small particle size in the range of nanometres, the particles are able to penetrate the respiratory system up to the lungs. This is on one hand dangerous because some particles cannot be removed from the lungs and can therefore cause an immunoreaction. On the other hand, if particles are able to reach the blood circuit, they can evoke systematic damages in other organs [8]. Till now, biological threats which originate from a large scale usage of nanoparticles are not completely understood and especially long term effects cannot be judged. Additionally, nanoparticles can accumulate in the environment with almost unknown implications in the future.

In fact, the evaluation of the environmental impacts of nanoparticles is the subject of numerous recent studies (e.g. [9, 10, 8]).

The process described here offers the possibility for the production of hydrophobic surfaces without the need of dangerous chemicals and without the need for the manipulation of potentially dangerous nanoparticles. The nano-scaled structure will be produced directly onto the surface of the sample and emission of nanoparticles can be reduced.

Moreover, it is expected that the process can be integrated into existing production lines easily. As a result, pollution of the environment is minimized as well as energy consumption of the process. In addition to the advantages mentioned already, economic feasibility will be increased, too.

## 2 Laser interference

As already mentioned, an ultra-short pulse laser system will be used for experiments. The system should have pulse duration in the sub picosecond range and a pulse frequency up to one MHz. Its fundamental wavelength will be 1064 nm. SHG and respectively THG modules allow the emission of the second or third harmonic wavelength, what results in minimized interference pattern sizes.

The periodic structures will be fabricated by the ablation of material caused by interference of laser radiation. Therefore the laser beam will be divided by optical elements into at least two partial beams which will be recombined at the surface of the material. The experimental set-up is described below.

From basic electromagnetic theory it is known that the total field strength of a combination of different electromagnetic fields is the sum of single field strengths. The resulting superposition of the field strengths of partial beams and since the intensity is proportional to the square of the field strength, $I \propto E^2$, the intensity includes interference terms:

$$E = \sum E_{0,i} \cdot \mathrm{e}^{-i(\vec{k_i}\cdot\vec{r}-\omega t+\phi_i)}. \quad (1)$$

The resulting intensity distribution depends on the wave vectors. Therefore the easiest way to manipulate the resulting structures is to change the angle between partial beams. Further manipulation can be achieved by change of the phase relations or the polarization of the partial beams [11].

Beam separation into two or more partial beams can be done by optical elements like mirrors or grids. Beam guidance is done by mirrors; phase relation of the partial beams can be done with beam delay slides. Fig. 1 and Fig. 2 show an example of a three-beam interference with the resulting intensity distribution.

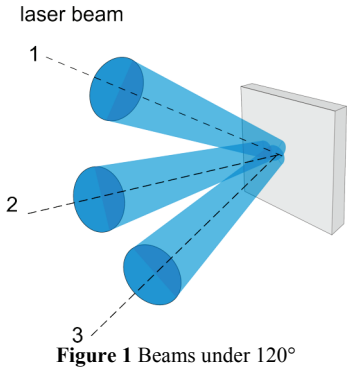


**Figure 1** Beams under 120°

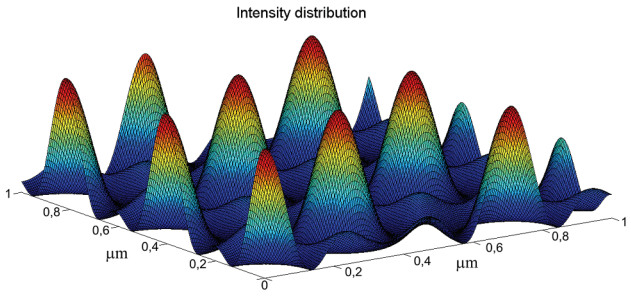


**Figure 2** Related intensity distribution

### 2.1 Two-beam interference

First experiments will be done with a two-beam interference set-up. These experiments will help to

identify the main parameters of the optical system and the laser system used for experiments. They will also help to find suitable methods for the evaluation of the produced structures.

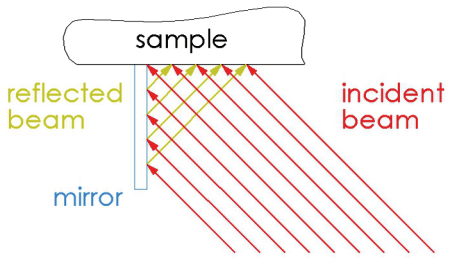


**Figure 3** Setup of Lloyds mirror

The easiest way of a two-beam interference is the Lloyds mirror [11, 12], where a part of a beam interferes with its own reflection. Figure 3 shows the principle set-up.

In general, every two beam interference results in a line shaped pattern. Periodicity of the resulting pattern can be easily calculated [12]:

$$P = \frac{\lambda}{2 \cdot \sin\theta}. \quad (2)$$

The production of grid shaped patterns can be achieved by two exposures, with a rotation of the sample in between.

### 2.2 Multi-beam interference

There are innumerable ways to establish multi-beam interference e.g. with the use of grids, mirrors and beam delay slides in order to change angle and phase relation of partial beams [13], or by the use of a prism, where the incident beam will be divided into four partial beams which interfere at the sample surface, according to Wu et al. [14, 15].

Independent of the solutions used, the diameter of the partial beams has to be as large as possible to provide a huge treatment area. It has been shown by Fucetola et al. and Byun that processing of areas in the range of some mm² up to cm² [16, 12] is possible.

The model presented in this paper is based on the so called diffractive variable delay generator (DVDG), presented by Klein-Wiele and Simon [11]. It consists mainly of two diffractive beam splitters followed by an aperture.

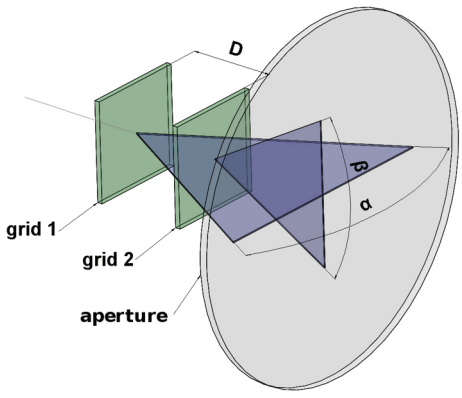


**Figure 4** Setup of the Diffractive Variable Delay Generator

Two gratings, which are placed perpendicular to each other act as a beam splitter. If the distance between them is adjustable, it is also possible to manipulate the phase relation between the two beam pairs. The angle between the partial beams is the result of the diffractive elements and the aperture.

## 3 Simulation

The simulations were done with the open source software Scilab, Version 5.3.3.

Resulting intensity distributions were calculated as well as expected ablation rates.

The simulation does not include polarization states or intensity distributions of the partial beams.

The ultra-short pulse Laser system which will be used for practical experiments has a fundamental wavelength of 1064 nm and the possibility of second (532 nm) and third (354,7 nm) harmonic generation.

Calculations of the resulting intensity distribution cover all three wavelengths, while simulation of the ablation result is just done for the third harmonic.

All simulations were done with a pulse length of 100 fs.

As a first step the Lloyds mirror has been simulated. After that the model was expanded by two beams and the possibility of a phase shift of each beam pair to represent the DVDG setup.

### 3.1 Intensity distribution

The resulting intensity distribution was calculated from the square of the electric field strength:

$$\boldsymbol{I} = \sum_{i=1}^{n} \epsilon \cdot c \cdot \boldsymbol{E}_i^2, \quad (3)$$

where $n$=2 in case of the Lloyds mirror and $n$=4 in case of the diffractive variable delay generator. Permittivity was calculated from $\epsilon = \epsilon_0 * \epsilon_r$ with $\epsilon_r = 2{,}4$ according to Clipper Controls® [17]. Speed of light is implied by $c^2 = \frac{1}{\epsilon \cdot \mu}$ with the permeability $\mu = \mu_0 \cdot \mu_r$. As material will be plastic, $\mu_r$ was set to 1. Partial electric fields include the interference terms:

$$\boldsymbol{E}_i = \boldsymbol{E}_{0,i} \cdot \cos\left(\vec{k_i} \cdot \vec{r} - \omega t + \Phi_i\right). \quad (4)$$

The considered wavelengths are inserted into the calculation through the wave vector $\vec{k}$, as its absolute value was set to $\frac{2\pi}{\lambda}$:

$$\vec{k_i} = \frac{2\pi}{\lambda} \cdot (x_i \quad y_i \quad z_i). \quad (5)$$

### 3.2 Ablation rate

A logarithmic ablation function was used to calculate expected ablation rates:

$$h = a^{-1} \cdot \ln\left(\frac{F}{F_t}\right), \quad (6)$$

where $h$ is the ablation depth, $a$ is the optical absorption coefficient and $F_t$ is the threshold fluence.

Absorption coefficients for various plastics could be found at Bäuerle [18]. Ruotsalainen measured ablation rates as well as ablation threshold for various materials [19]. All ablation simulations were done with Polyethylene terephthalate. Absorption coefficient and threshold fluence are shown in Tab. 1:

**Table 1** Optical absorption coefficient and ablation fluence

| Material | a / $cm^{-1}$ | $F_t$ / mJ/cm² |
|---|---|---|
| PET | $4\times10^3$ | 30 |

The absorption coefficient is strongly depended on the wavelength. In this case $a$ was measured at 308 nm and is therefore valid just for the third harmonic wavelength.

## 4 Results

### 4.1 Lloyds mirror

The model consists mainly of two beams which propagate in the $x$-$y$ layer. The angle between sample and beam propagation direction has been defined with 45° in one simulation and 60° in the other. As the model is symmetric, the angle between mirror and beam propagation direction is the same.

The position vector goes from 0 to 1 µm in $x$- and $y$-direction; $z$-direction was set to 0.

Figs. 5 to 7 show the resulting intensity distribution with the first, second and third harmonic wavelength and an angle of 90° between incident and reflected beam. The decreasing wavelength results in decreasing feature sizes:

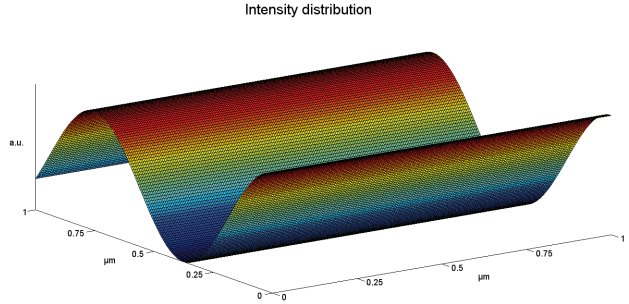


**Figure 5** Intensity distribution for $\alpha$=90°, $\lambda$=1064 nm

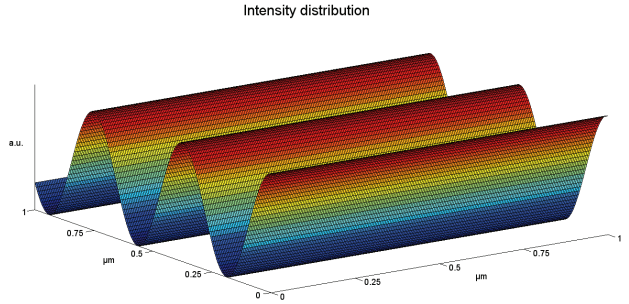


**Figure 6** Intensity distribution for $\alpha$=90°, $\lambda$=532 nm

Figure 8 shows the expected ablation result of the third harmonic wavelength. Width of the strips is about 125 nm. Ablation depth is about 2,5 µm.

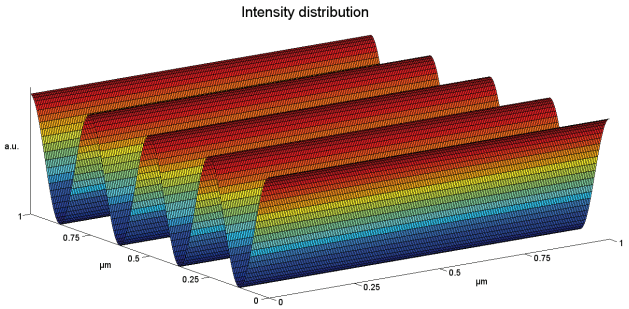


**Figure 7** Intensity distribution for $\alpha$=90°, $\lambda$=354,7 nm

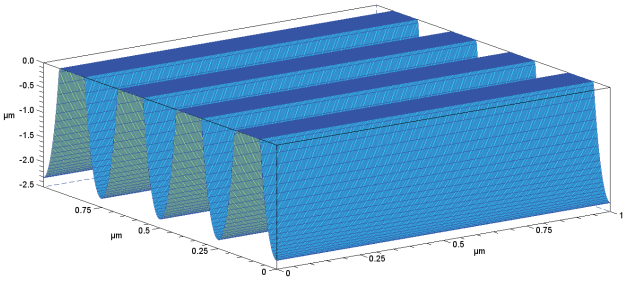


**Figure 8** Ablation result for PET, $\alpha$=90°, $\lambda$=354,7 nm

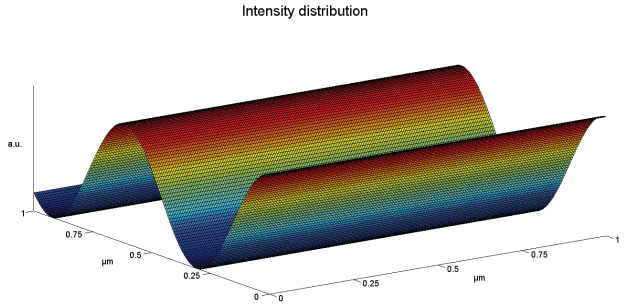


**Figure 9** Intensity distribution for $\alpha$=120°, $\lambda$=1064 nm

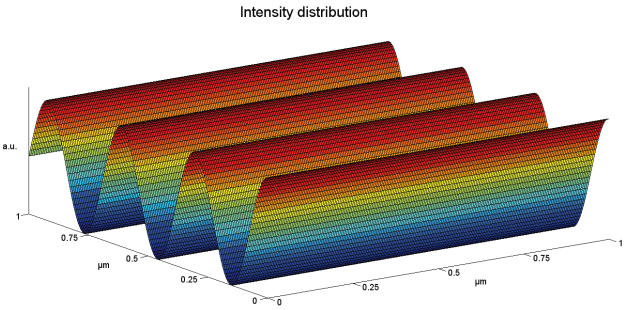


**Figure 10** Intensity distribution for $\alpha$=120°, $\lambda$=532 nm

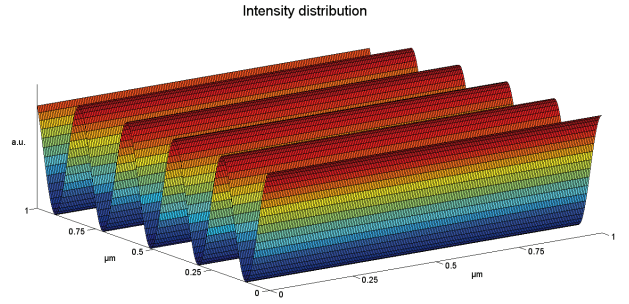


**Figure 11** Intensity distribution for $\alpha$=120°, $\lambda$=354,7 nm

The larger angle between the partial beams decreases the distance between the characteristic lines, the smaller one increases it and also results in a lower intensity, as the exposed area increases. Figure 9 to Figure 11 show the

resulting intensity distribution with the first three harmonic wavelengths with an increased angle of 120° between incident and reflected beam.

Figure 12 again shows the ablation result. By increasing the angle between the partial beams, width of the strips could be decreased to about 100 nm.

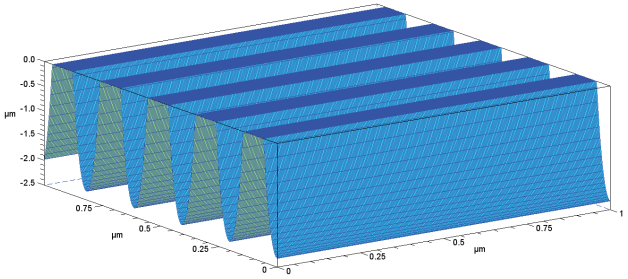

**Figure 12** Ablation result for PET, $\alpha$=120°, $\lambda$=354,7 nm

## 4.2 Diffractive variable delay generator

The second model shows the possibilities of the diffractive variable delay generator.

In the first case, the simplest experimental set-up has been simulated: two perpendicular pairs of beams without phase shift. First simulation has been done with an angle of 90° between the partial beams of each pair, the second simulation with an angle of 120°. Both configurations have been simulated with the first three harmonic wavelengths. Position vector again goes from 0 to 1 µm in $x$- and $y$-direction.

Figure 13 shows the resulting intensity distribution for an angle of 90° between the beams of both beam pairs.

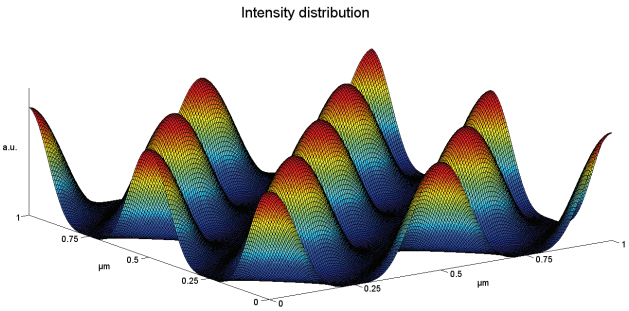


**Figure 13** Intensity distribution for $\alpha$=90°, $\beta$=90°, $\lambda$=354,7 nm

Figure 14 shows the according ablation result. Diameter of the holes is about 200 nm, ablation depth is about 2,5 µm.

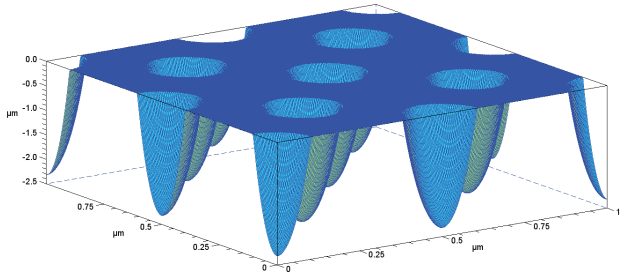

**Figure 14** Ablation result for PET, $\alpha$=90°, $\beta$=90°, $\lambda$=354,7 nm

Figure 15 shows the possibilities of asymmetric beam pairs; the first beam pair again has an angle of 90°, the second beam pairs an angle of 40°.

This modification results in ellipsoid features with a length of the principle axis of about 500 nm and a length of the minor axis of about 200 nm.

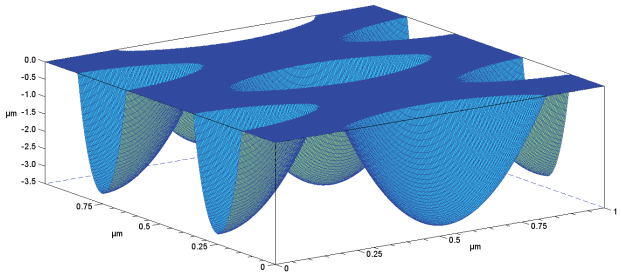

**Figure 15** Ablation result for PET, $\alpha$=90°, $\beta$=40°, $\lambda$=354,7 nm

Next calculation goes one step further: A phase shift of $\theta = \frac{\pi}{2}$ for the second beam pair was calculated, which results in this case in a mixture of a stripped and an ellipsoid pattern.

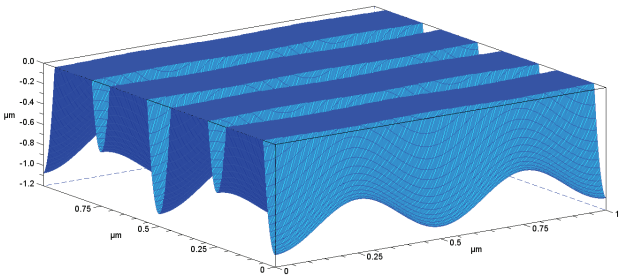

**Figure 16** Ablation result for PET, $\alpha$=90°, $\beta$=90°, $\theta$=$\pi$/2, $\lambda$=354,7 nm

Further feature shapes are possible, if the beam pairs are not perpendicular to each other. In Figure 17 and Figure 18 the layer of the second beam pair is shifted about 45° to the layer of the first pair. This results in a periodic super lattice.

Simulation shown in Figure 17 is done without a phase shift, Fig. 18 was again done with a phase shift of $\theta = \frac{\pi}{2}$.

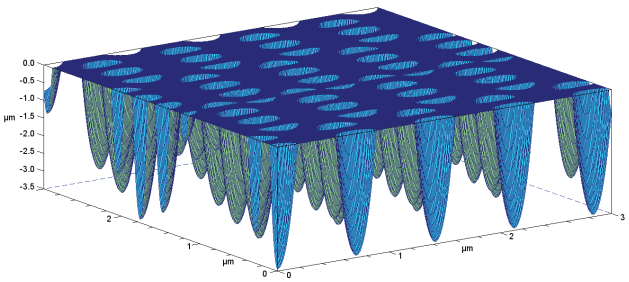

**Figure 17** Ablation result for PET, $\alpha$=90°, $\beta$=90°, $\gamma$=45°, $\lambda$=354,7 nm

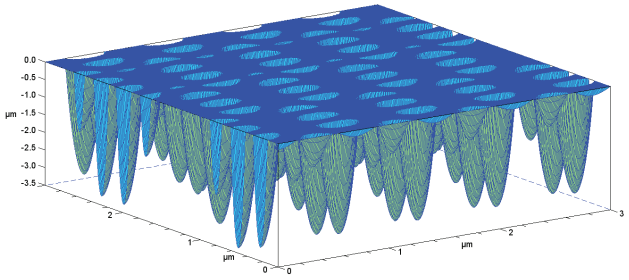

**Figure 18** Ablation result for PET, $\alpha$=90°, $\beta$=90°, $\gamma$=45°, $\theta$=$\pi$/2, $\lambda$=354,7 nm

## 5 Discussion and outlook

Simulations show the feasibility of the fabrication of nanostructures in order to create a lotus-effect by multi-beam interference of ultra-short laser pulses.

As the simulation results with the Lloyds mirror indicate, it seems possible to produce line-like structures with a width of about 100 nm, depending on wavelength and interference angle. A rotation of the sample after the exposure and a subsequent exposure should induce a grid shaped structure with a mesh size of about 100 × 100 nm. The model has to be extended to demonstrate this.

Simulation results achieved based on the model of the diffractive variable delay generator indicate that the fabrication of a grid with a mesh size of 200 × 200 nm in one step is possible.

Furthermore, there are innumerable feature shapes which can be achieved by different angles and phase relations between the partial beam pairs.

The model can easily be extended by additional partial beams, which results in different features and feature sizes of the pattern.

Further considerations and simulations are necessary to estimate possible structures and their consequences on the wetting behaviour of samples. Till now, polarization states as well as intensity distributions of real laser beams are not considered in simulations presented here. Additional work has to be done to include all mentioned features.

Nevertheless, results indicate a promising possibility for the production of nano-sized structures.

The next step, experimental verification of simulation results, is of utmost importance.

## 6 References

[1] Neinhuis, C.; Barthlott, W. Characterization and Distribution of Water-repellent, Self-cleaning Plant Surfaces. // Annals of Botany, 97(1997), pp. 667–676.

[2] Wagner, T.; Neinhuis, C.; Barthlott, W. Wettability and Contaminability of Insect Wings as a Function of Their Surface Sculptures. // Acta Zoologica, 77, 3(1996), pp. 213–225.

[3] Jopp, K. E. Nanotechnologie - Aufbruch ins Reich der Zwerge. 2nd ed. Wiesbaden: Gabler, 2006.

[4] Martines, E.; Seunarine, K.; Morgan, H.; Gadegaard, N.; Wilkinson, C. D. W.; Riehle, M. O. Superhydrophobicity and Superhydrophilicity of Regular Nanopatterns. // Nano Lett, 10, 5(2005), pp. 2097–2103.

[5] Feng, L.; Li, S.; Li, H.; Zhai, J.; Song, Y.; Jiang, L.; Zhu, D. Super-Hydrophobic Surface of Aligned Polyacrylonitrile Nanofibers. // Angew. Chem. Int. Ed, 41, 7(2002), pp. 1221–1223.

[6] Rouette, H. Handbuch Textilveredlung. 15th ed. Frankfurt am Main: Dt. Fachverl, 2006.

[7] Platzek, T. Gesundheitsgefährdung durch Bekleidungs-textilien. // Bundesgesundhbl, 40, 7(1997), pp. 238–240.

[8] Wörle-Knirsch, J. M.; Krug, H. F. Risikoforschung und toxikologische Bewertung von Nanomaterialien. // Nano Lett, 1(2007), pp. 101–114.

[9] Committee to Review the National Nanotechnology Initiative NRC. A matter of size: Triennial review of the National Nanotechnology Initiative. Washington, D. C.: National Academies Press, 2006.

[10] Klien, K. The genotoxic effects of FeCoB nanoparticles on human fibroblasts assessed by comet assay. Master's Thesis. Med. Univ. Wien, 2010.

[11] Klein-Wiele, J.; Simon, P. Fabrication of periodic nanostructures by phase-controller multiple-beam interference. // Applied Physics Letters, 83, 23(2003), pp. 4707–4710.

[12] Byun, I.; Kim, J. Cost-effective laser interference lithography using a 405 nm AlInGaN semiconductor laser. // J. Micromech. Microeng, 20, 5(2010), pp. 1-6.

[13] Mannini, M.; Tisserand, S.; Peng, C.; Olaizola, S. M. DELILA Report: Development of Lithography Technology for Nanoscale Structuring of Materials Using Laser Beam Interference. 2006. URL: http://www.docstoc.com/docs/70759985/DELILA-D31pdf---DELIVERABLE-D31-Requirement-analysis-DELILA. (05.08.2012).

[14] Wu, L.; Zhong, Y.; Chan, C. T.; Wong, K. S.; Wang, G. P. Fabrication of large area two- and three-dimensional polymer photonic crystals using single refracting prism holographic lithography. // Applied Physics Letters, 86, 24(2005), pp. 2411021–23.

[15] Lei, M.; Yao, B. Structuring by multi-beam interference using symmetric pyramids. // Optics Express, 14, 12(2006), pp. 5803–5811.

[16] Fucetola, C. P.; Korre, H.; Berggren, K. K. Low-cost interference lithography. // Journal of Vacuum Science & Technology B: Microelectronics and Nanometer Structures, 27, 6(2009), pp. 2958–2961.

[17] Clipper Controls. Dielectric Constant Values. 2012. URL: http://www.clippercontrols.com/pages/Dielectric-Constant-Values.html. (05.08.2012).

[18] Bäuerle, D. Laser processing and chemistry. 2nd ed. Berlin, New York: Springer. 1996.

[19] Ruotsalainen, S.; Laakso, P.; Penttilä, R.; Pantsar, H. Picosecond Laser Processing – Material Removal Rates of Plastics. // Proceedings of the 11th NOLAMP Conference Nordic Laser Materials Processing Conference, 2007.

**Authors' addresses**

***Pospichal Robert***
Vienna University of Technology
Institute for Production Engineering and Laser Technology
Gusshausstraße 30
1040 Vienna, Austria
E-mail: robert.pospichal@tuwien.ac.at

***Liedl Gerhard, Ao. Univ. Prof. Dipl.-Ing. Dr. techn.***
Vienna University of Technology
Institute for Production Engineering and Laser Technology
Gusshausstraße 30
1040 Vienna, Austria
E-mail: gerhard.liedl@tuwien.ac.at